Aliphatic polyketone-based thin film composite membrane with mussel-inspired polydopamine intermediate layer for high performance osmotic power generation

Ralph Rolly Gonzales [ab], Lei Zhang [c], Kecheng Guan [b], Myoung Jun Park [a], Sherub Phuntsho [a], Ahmed Abdel-Wahab [d], Hideto Matsuyama [b,c*], Ho Kyong Shon [a*]

[a] *Centre for Technology in Water and Wastewater, University of Technology Sydney, New South Wales, Australia*

[b] *Research Center for Membrane and Film Technology, Kobe University, Kobe, Hyogo, Japan*

[c] *Department of Chemical Science and Engineering, Kobe University, Kobe, Hyogo, Japan*

[d] *School of Chemistry and Chemical Engineering, Shandong University of Technology, Zibo, China*

[e] *Chemical Engineering Program, Texas A & M University at Qatar, Education City, Doha, Qatar*

* Corresponding author; Email: matuyama@kobe-u.ac.jp; hokyong.shon-1@uts.edu.au

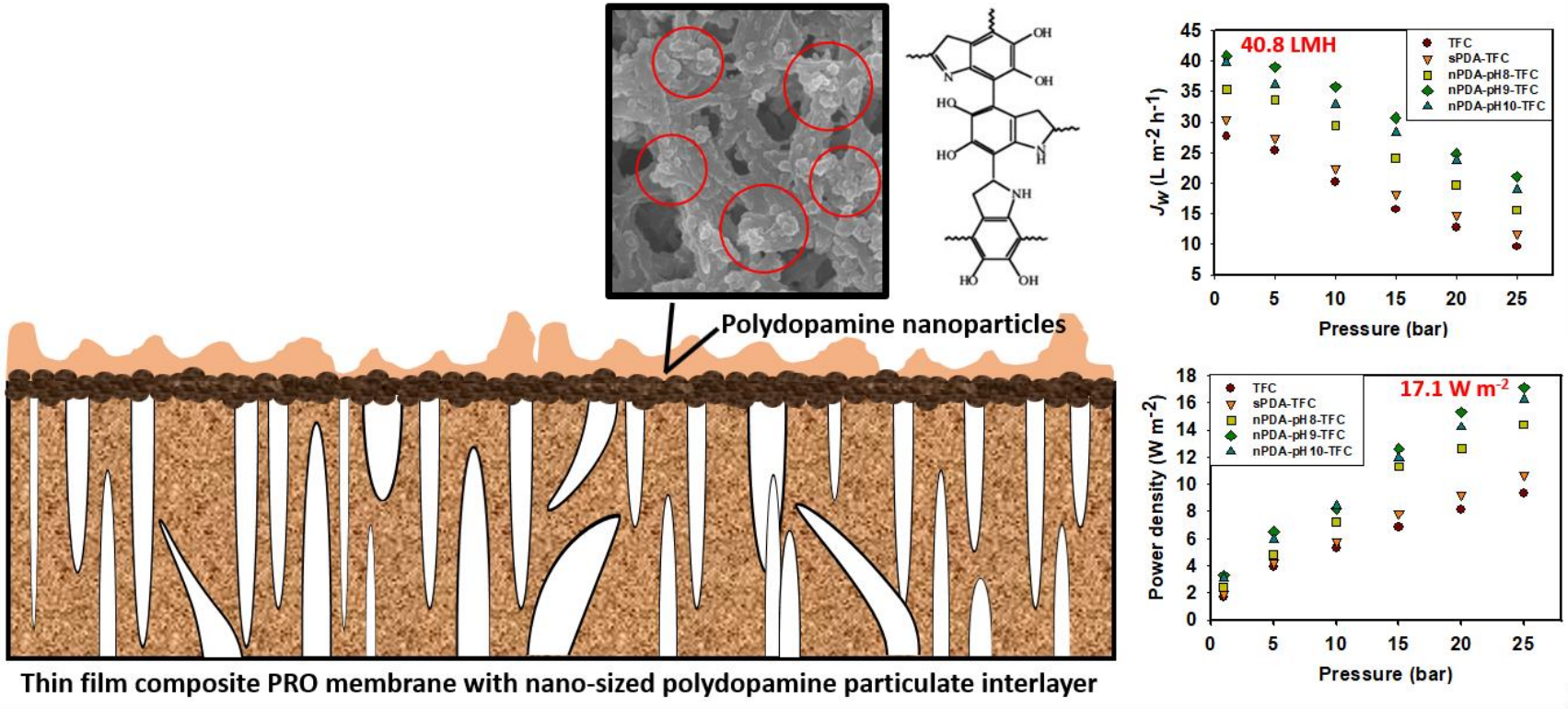
Polydopamine nanoparticles
Thin film composite PRO membrane with nano-sized polydopamine particulate interlayer
40.8 LMH
TFC
sPDA-TFC
nPDA-pH8-TFC
nPDA-pH9-TFC
nPDA-pH10-TFC
J_w (L m^{-2} h^{-1})
Pressure (bar)
17.1 W m^{-2}
Power density (W m^{-2})
Pressure (bar)

12

Abstract

Polydopamine (PDA), formed from self-polymerization of dopamine, was coated on aliphatic polyketone membrane substrate prior to interfacial polymerization (IP), preparing a pressure retarded osmosis (PRO) thin film composite (TFC) membrane with a PDA interlayer. The effect of the formation of two types of PDA interlayers — smooth and particulate — on substrate morphology, polyamide formation, and PRO osmotic performance were investigated. Also, the effect of pH on the particulate PDA interlayer was studied. It was found that the introduction of both smooth and particulate PDA contributes to enhanced water flux and power density of the PRO membranes. pH was found to have significantly affected the formation of particulate PDA and the polyamide formation, as well. At higher pH, PDA self-polymerization led to the formation of more nanoparticles, the subsequent increase in surface roughness and decline in the polyketone substrate porosity. The particulate PDA interlayer formed looser polyamide, compared to the thinner and denser polyamide formed on pristine and smooth PDA-interlayer-coated TFC membranes. The membrane performance was evaluated using deionized water and 1.0 M NaCl as feed and draw solutions, respectively. The TFC membrane with nanoparticulate PDA layer formed at pH 9.0 exhibited the best initial water flux of 40.8 L m^{-2} h^{-1}, and this membrane also showed the highest power density of 17.1 W m^{-2} at 25 bar. The results of this study indicate that nanoparticulate PDA interlayer formation is a simple and scalable TFC membrane development method for engineered osmosis.

Keywords: Pressure retarded osmosis; Thin film composite membrane; Polydopamine; Osmotic power generation; Interlayer

1. Introduction

Currently, alternative sources of energy are needed to augment the world's continuously increasing energy requirements due to increased population and advanced economic development [1]. Until present, most of the earth's energy is obtained from vastly depleting fossil fuel reserves, which also causes greenhouse gas emissions giving rise to global warming and climate change. As a result of this energy crisis, scientific research from all over the world has looked into the following more sustainable energy sources: solar, wind, geothermal, biomass, and osmotic power [1-3].

Generation of osmotic power by means of pressure retarded osmosis (PRO) is achieved due to the natural occurrence of osmosis between two solutions of varying salinity levels and osmotic pressures with a semi-permeable membrane separating each solution [4, 5]. The difference in osmotic pressure allows water permeation from the feed solution (FS), whose concentration is lower, toward the pressurized higher concentrated draw solution (DS). Osmotic power can then afterwards be harvested by delivering the pressurized DS to a hydro turbine, which produces electrical energy [6].

Alongside the development of PRO as a commercially-viable and technologically-feasible process is the manufacture of membranes specifically tailored for PRO application. Recently, research on PRO membrane development has shown a tangible progress, especially for the manufacture of thin film composite (TFC) membranes with high power density.

TFC membranes are consisted of a membrane substrate with high porosity and a dense thin film selective layer, typically polyamide, formed atop the porous substrate through interfacial polymerization (IP). In the previous studies, efforts were made to engineer TFC PRO membranes using a variety of methods [7, 8], modifying agents [9-11], and nanomaterial fillers [12, 13]. These techniques were aimed at improving the water permeability, selectivity, and mechanical strength of the membranes, in order to improve overall osmotic power generation performances.

Among the chemical agents used in modifying PRO TFC membranes is polydopamine (PDA) [14]. This polymer is formed from the self-polymerization of dopamine (3,4-dihydroxyphenylalanine) in alkaline conditions. The properties of PDA are known to be similar to the phenolic protein that are found in mussels, causing PDA to be called a bio-inspired or mussel-inspired material. PDA is mainly used for coating a wide range of materials, from nanomaterials to huge surfaces, and it is also widely used as an adhesive. PDA is highly hydrophilic, owing to the presence of hydrophilic hydroxyl and amine groups. Therefore, this polymer has been used for modification of membranes utilized in water-based technologies to enhance separation performance and even fouling resistance [15, 16]. PDA has become a versatile and efficient engineering agent in membrane development, and it can be applied on membranes using any of the following techniques: (a) surface deposition [17], (b) addition in polymer dope solution prior to casting [18], (c) covalent linkage with other molecules by exploitation of Michael or Schiff base reactions [19], and (d) intermediate layer formation [20]. PDA has been widely used to facilitate the formation of intermediate layer and reinforce the incorporation of amphoteric substances [21] and nano-sized inorganic fillers, such as graphene oxide [22], silica [23], taurine-modified hydroxyapatite [24], halloysite nanotubes [25], and covalent organic framework [26].

Recent studies have revealed the formation of nano-sized PDA particles when, instead of Tris-HCl buffer, ammonia is used to initiate the dopamine self-polymerization [20]. This method is different from the conventional PDA modification which uses an aqueous PDA and Tris-HCl buffer solution on the surface to form a smooth film. In this study, both smooth and particulate PDA interlayers were formed between an aliphatic polyketone substrate and the selective polyamide layer. Furthermore, it has been long established that the catechol and amine groups present in PDA can react with the acyl chloride precursor during IP. The introduction of a PDA interlayer between the membrane substrate and selective layer has been found to facilitate excellent formation of mechanically-strong thin film, as caused by the adhesive properties of PDA.

The introduction of nanomaterials in TFC membranes for PRO has led to a new class of membranes known as thin film nanocomposite (TFN) membranes. PRO TFN membranes have been developed by incorporating nano-sized materials, like graphene oxide [27], covalent organic framework [12], porous polymer [13], carbon quantum dots [28, 29], and carbon nanotubes [30], either in the membrane substrate or the polyamide selective layers. TFN membranes have exhibited enhanced water permeability, mainly caused by the presence of the highly porous and hydrophilic nanomaterials. Nanomaterial incorporation in the intermediate layer between the substrate and selective layers of PRO TFC membranes has not yet fully been explored, and this study aims to exploit nano-sized particulate PDA as an intermediate media for PRO TFC membranes.

This study aimed to discover whether the formation of particulate PDA interlayer could retain the high permselectivity of the pristine TFC and TFC membrane with smooth PDA interlayer, and how the interlayer structure could affect polyamide formation and the subsequent PRO operation performance. Furthermore, ammonia-initiated polymerization of dopamine was also investigated in terms of varying alkaline pH. While research on TFC membrane modification using PDA has been abound, this manuscript provides insight on how changes in polymerization agent and alkalinity could influence a technique as simple as PDA modification and the PRO performance, as well.

2. Experimental

2.1. Chemicals

The membrane substrate was prepared using aliphatic polyketone (PK, M_w = 200000 g mol^{-1}, Asahi Kasei Co., Japan) and polyester (PET) nonwoven fabric (90HP, Awa Seishi Co., Japan). To prepare the PK polymer dope solution, resorcinol (> 99.0%) and deionized (DI) water were used as solvents. Acetone (> 99.8%) and hexane (> 99.8%) were used during flat sheet membrane casting. Membrane modification was conducted using dopamine hydrochloride (dopamine HCl), Tris(hydroxymethyl) aminomethane (Tris),

104 hydrochloric acid (HCl, 1 mol L^{-1}), ammonia (25.0~27.9%, in solution), and ethanol (99.5%). *m*-
105 phenylenediamine (MPD), trimesoyl chloride (TMC, > 98.0 %), (±)-10-camphorsulfonic acid (CSA, >
106 98.0 %), sodium dodecyl sulfate (SDS), triethylamine (TEA, > 99.0 %), and heptane (> 99.3 %) were used
107 for interfacial polymerization. Sodium chloride (NaCl) was used for membrane osmotic performance
108 testing. Resorcinol, TMC, and CSA were supplied by Tokyo Chemical Industry Co., Ltd., Japan. Dopamine
109 HCl and Tris were supplied by Sigma-Aldrich, Japan. Lastly, acetone, hexane, HCl, ammonia, ethanol,
110 MPD, TEA, SDS, heptane, and NaCl were supplied by Fujifilm Wako Pure Chemical Corp., Japan.

111 All the reagents used in this study were used without further treatment.

112

113 ***2.2. Membrane preparation***

114 ***2.2.1. Membrane casting and polydopamine interlayer formation***

115 Flat sheet PK membrane substrate was fabricated by conventional nonsolvent-induced phase
116 separation (NIPS). First, a 10 wt% PK solution was prepared by dissolution of the polymer into a
117 resorcinol/DI water (65:35) solvent mixture at 80℃ with constant stirring. Ahead of casting, the polymer
118 solution was degassed at 50℃ overnight. The solution was poured onto a glass plate and was spread with
119 a casting thickness of 400 μm using a stainless-steel casting knife. The PK film was afterwards immersed
120 in a 35% aqueous methanol coagulation bath for 20 min for phase separation to occur. The membrane
121 substrate was then placed in steel frames to avoid shrinkage before successive 20 min immersion cycles in
122 acetone and hexane baths. The membrane substrate was air-dried afterwards until further use.

123 A polydopamine (PDA) interlayer was formed *in situ* on the top side of the PK membrane substrate.
124 Two types of PDA interlayer were formed: the conventional smooth PDA and the nano-sized particulate
125 PDA, afterwards denoted as PK-sPDA and PK-nPDA, respectively.

126 The typical smooth PDA layer formation method required 2 mg mL^{-1} of dopamine HCl dissolved in
127 a 0.01 M Tris-HCl solution (pH 8.5). The membrane substrate surface was immersed in the solution for 8
128 h while agitating at 400 rpm using a shaker (Eyela, Japan) in room temperature [31].

129 For the formation of particulate PDA interlayer, a 2 mg mL^{-1} dopamine HCl was dissolved in an
130 aqueous 30% (v/v) ethanol solution [20]. The pH of the solution was adjusted to 8,9, and 10 by adding 25%
131 ammonia solution dropwise, corresponding to PK-nPDA-pH8, PK-nPDA-pH9, and PK-nPDA-pH10,
132 respectively. The membrane substrate surface was immersed in the solution for 8 h at light agitating
133 conditions.

134 All PDA-coated membrane substrates were washed with copious DI water prior to interfacial
135 polymerization.

136

137 ***2.2.2. In situ selective polyamide layer formation via interfacial polymerization***

138 The selective polyamide thin film layer was constructed *in situ* on top of the PDA-coated PK
139 substrate by interfacial polymerization (IP) reaction between MPD and TMC. The membrane substrate was
140 initially submerged for 5 min in an aqueous 2 wt% MPD solution, which also contains the following: 2.3
141 wt% CSA, 1.1 wt% TEA, and 0.15 wt% SDS. The excess solution was drained and completely eliminated
142 using an air knife, prior to 2 min immersion of the membrane substrate in 0.15 wt% TMC in hexane solution.
143 The membrane was then cured at 90℃ for 10 min. The TFC membrane was afterwards washed with and
144 stored in DI water.

145

146 ***2.3. Determination of intrinsic transport parameters and evaluation of membrane osmotic performance***

147 The membrane intrinsic transport properties, pure water permeability constant (A, L m^{-2} h^{-1} bar^{-1}) and
148 solute permeability constant (B, L m^{-2} h^{-1}), were determined using a cross-flow reverse osmosis (RO) system

[32] whose membrane cell has an effective membrane area (A_m) of 8.07 cm^2, under a pressure of 10 bar, a flow rate of 150 mL min^{-1}, and temperature of 25°C. DI water and 1000 mg L^{-1} NaCl were used as the feed for determination of *A* and *B*, respectively.

The TFC membranes were evaluated for PRO performance using a bench-scale system [33]. DI water and 1.0 M NaCl were respectively used as the FS and DS. The system consists of a stainless-steel membrane cell (Nitto Denko C-70F), whose effective membrane area is 38.15 cm^2. The cell was equipped with a tricot spacer to facilitate flow of the FS and a metal plate with hole openings was positioned to lessen the contact of the membrane with the cell wall. The FS was delivered with a flow rate of 100 mL min^{-1} using a plunger-style pump system (NP-KX-840, Nihon Seimitsu Kagaku, Japan), while the DS was delivered and pressurized using a high-pressure diaphragm pump (Hydra-Cell, Wanner Engineering Inc., Japan) with a flow rate of 600 mL min^{-1}. The changes in mass and conductivity of the FS were monitored during the PRO operation.

Water flux (J_w, L m^{-2} h^{-1}) and the *A* value can be calculated using the following:

$$J_w = \frac{\Delta V}{A_m \Delta t} \quad (1)$$

$$A = \frac{J_w}{\Delta P} \quad (2)$$

where ΔV, A_m, Δt, and ΔP are the permeate volume (L), membrane area (m^2), operation time (h), and difference in transmembrane pressure (bar), respectively [34]. Using changes in volume and conductivity, the solute rejection (*R*) and *B* value can be calculated using the following equations:

$$R = \left(1 - \frac{C_p}{C_f}\right) x\ 100\% \quad (3)$$

$$B = \left(\frac{1-R}{R}\right)(\Delta P - \Delta\pi)A \quad (4)$$

where C_f, C_p, and $\Delta\pi$ are the salt concentration of the feed, salt concentration of the permeate, and transmembrane osmotic pressure difference, respectively. Reverse salt flux (J_s, g m^{-2} h^{-1}) is determined using the concentration changes (C_f) and feed solution volume (V_f) at time *t*, according to the following equation:

$$J_s = \frac{\Delta(C_f V_f)}{A_m \Delta t} \quad (5)$$

Using J_w and the hydraulic pressure applied ΔP, the power density W can be calculated using this equation:

$$W = J_w \Delta P \quad (6)$$

The membrane structure parameter, S, can be calculated from the following equation:

$$J_w = \frac{D}{S} \ln \frac{A \times \pi_D + B}{A \times \pi_F + J_w + B} \quad (7)$$

where π_D and π_F are the respective osmotic pressures of the draw and feed solutions, and D is the solute coefficient [4, 12].

2.4. Membrane characterization

Membrane surface and cross-sectional structure was imaged and characterized using field-emission scanning electron microscopy (FE-SEM, JSF-7500F, JEOL, Japan). Prior to imaging, the samples were dried overnight using a freezer drier (FD-1000, EYELA, Japan), and were sputter-coated with osmium with 10 nm thickness. Measurements were done in triplicate. Surface pore size was measured from the FE-SEM images using ImageJ image processing software (National Institute of Health, USA).

Surface chemistry was characterized using Fourier transform infrared spectroscope (FTIR, Nicolet iS5, Thermo Fisher Scientific, Japan) with an attenuated total reflectance (ATR) detector (iD5, Thermo Fisher Scientific, Japan), and X-ray photoelectron spectroscopy (XPS, JPS-9010 MC, JEOL, Japan) using Al Kα X-rays.

The bulk porosity of the membrane substrates was measured using gravimetric method; the support was initially soaked in ethanol for 12 h [35]. A capillary flow porometer (CFP-1500AXLC, Porous Materials Inc., USA) was used to determine the membrane pore size. The membrane was initially soaked in a wetting liquid, Galwick® prior to porosity measurement.

The membrane hydrophilicity was evaluated by an optical contact angle instrument (Drop Master 300, Kyowa Interface Science Co., Japan) [36]. Water static contact angle measurements were obtained

after dispensing a 4 µL water droplet onto the membrane sample. Surface roughness was measured through an atomic force microscope (AFM, SP13800N/SPA400, SII Co., Japan) in tapping mode.

3. Results and discussion

3.1. Polydopamine modification and formation of smooth and nanoparticle polydopamine interlayer

Figure 1 shows the FTIR spectra of the membrane substrates, comparing the plain polyketone with the smooth and particulate PDA-coated ones. Peaks at 1705 cm^{-1} correspond to the PK substrate, as evidently seen from all samples. All the PDA-coated membrane substrates exhibited peaks attributed to the presence of PK and PDA groups, indicating the successful incorporation of the PDA interlayer. The peaks at around 1020 and 1350 cm^{-1} correspond to the C=C groups, while vibrations around 1600 cm-1 correspond to N-H group, indicating that PDA was formed during the self-polymerization of dopamine [35]. There was no substantial difference from the FTIR spectra of the membranes coated with PDA, whether smooth or particulate.

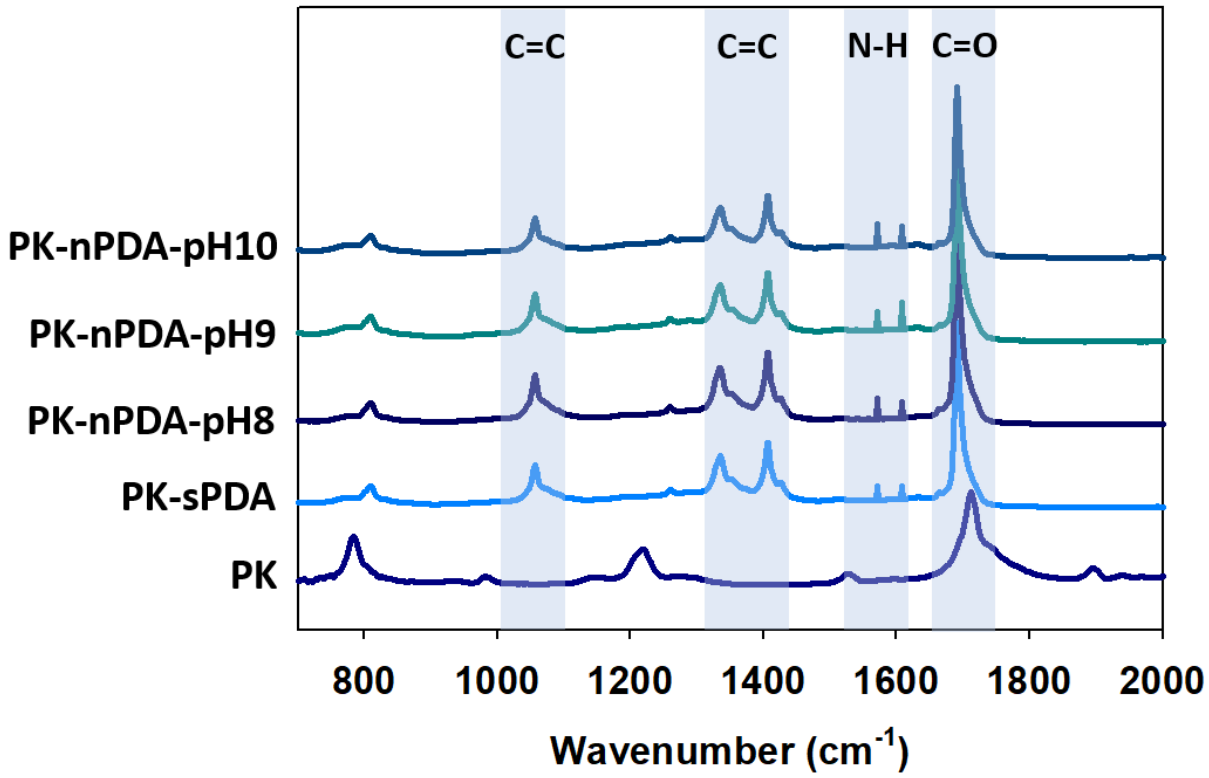

211

212 Figure 1. FTIR spectra of the pristine polyketone and PDA-modified membrane substrates.

213

214 To further analyze the surface chemistry of the PDA-coated membrane substrates, XPS analysis was
215 performed, and the elemental XPS analysis results are shown in Table 1. The elemental composition of the
216 membrane substrate surface confirms that there was indeed the presence of the PDA coating on top of the
217 polyketone, as evidenced by the increase in N content, starting from zero in pristine polyketone to the
218 5.28 % N content of the membrane substrate modified with PDA at pH 10. The self-polymerization of
219 dopamine to polydopamine is highly controlled by the pH of the reaction medium, with OH^- ions acting as
220 the catalyst. Typically, the pH of the self-polymerization reaction is controlled using a buffer to ensure the
221 gradual polymerization and facilitate the formation of a smooth polydopamine coating onto a surface. In
222 the case of this study, the self-polymerization was catalyzed by ammonia, and the pH of the solution

influenced the reaction. At lower pH (pH 8), the self-polymerization reaction was not fully catalyzed, as the reaction mostly takes place between pH 8.5 to 9, thus the dopamine which has not polymerized during the reaction period might have been washed off from the membrane surface, resulting in a lower N content, as seen from the XPS characterization, indicating the presence of less polydopamine on the membrane substrate surface. The higher reaction pH of the succeeding samples ensured that the self-polymerization reaction took place and resulted in the formation of the PDA nanoparticles which were embedded within the membrane substrate, and led to higher N content.

The morphology of the membrane substrates characterized using FE-SEM are shown in Figure 2. In general, PDA modification leads to enhancement of hydrophilicity and smoothness of the surface. However, in this study, it could be seen that while hydrophilicity was definitely enhanced upon introduction of the PDA interlayer [14], surface smoothness was only achieved when the conventional PDA modification technique was performed (Figure 2(b)). The smooth PDA interlayer appeared to be a smooth coating on the fibril-like structures of polyketone, still revealing the intrinsic highly porous structure of the membrane substrate. In the case of PDA nanoparticle formation as an interlayer, the roughness of the membrane substrate was observed to increase as pH increased (Figure 2(c)-2(e)). The particulate PDA interlayer was shown to exhibit granular surface with open pore structure. As the pH of dopamine self-polymerization reaction increased, there was an observed increase in the presence of particulate PDA structure attached onto the fibrous polyketone substrate. The nPDA-pH10 substrate has clearly shown aggregation of the PDA nanoparticles, which was known to be more prevalent at elevated pH [20], thus self-polymerization of dopamine is not performed at pH values higher than 10.

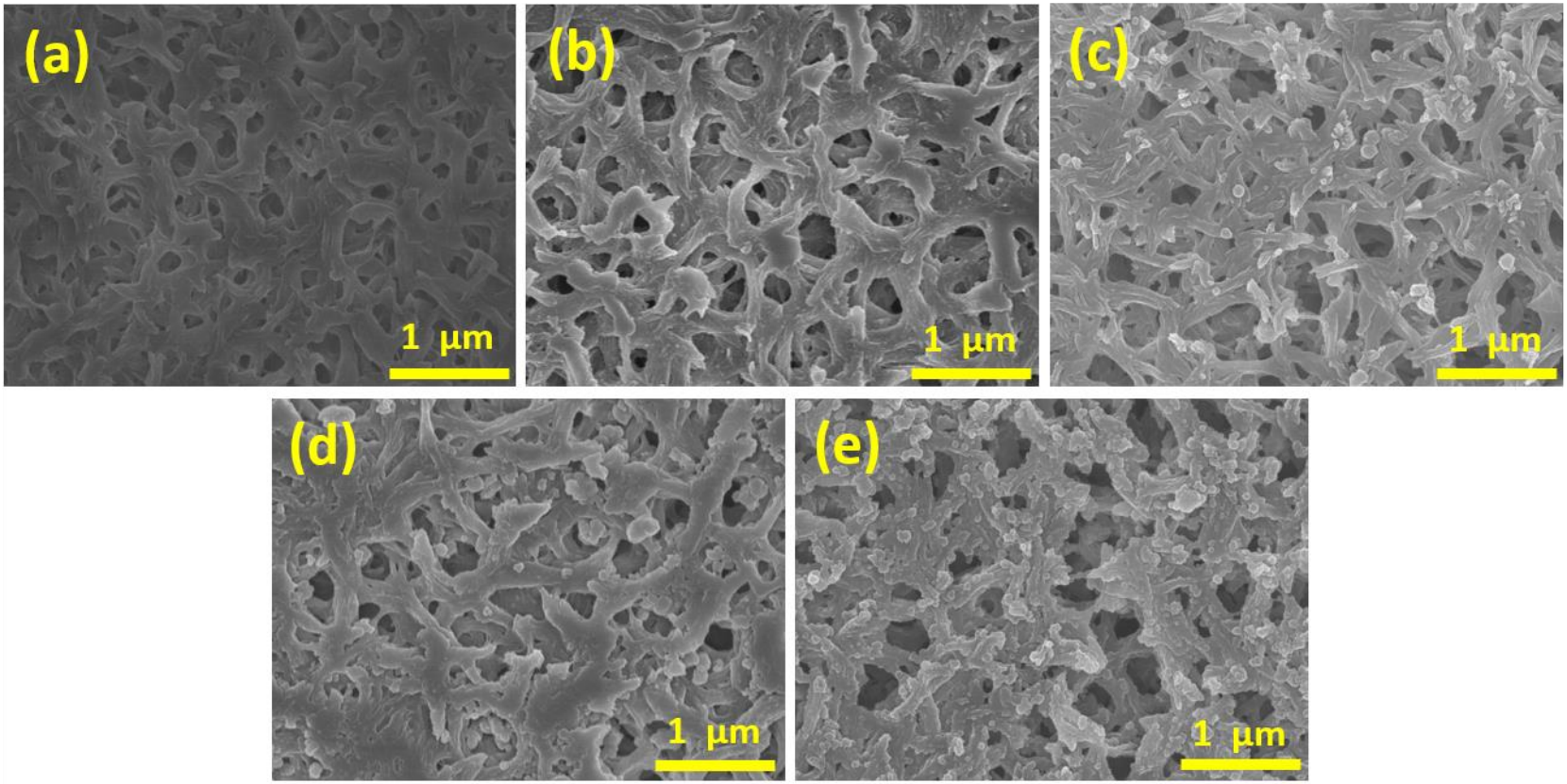

243

244 Figure 2. Surface morphology of the (a) pristine polyketone and PDA-coated membrane substrates: (b) sPDA, (c) nPDA-pH8, (d) nPDA-pH9, and
245 (e) nPDA-pH10.

Table 1. Surface elemental analysis of the PDA intermediate layer using X-ray photoelectron spectrometry.

Membrane substrate	C (%)	N (%)	O (%)	Others (%)
Polyketone	70.6	-	29.0	0.4
sPDA	72.3	3.1	24.3	0.3
nPDA-pH8	71.9	2.8	25.0	0.3
nPDA-pH9	73.9	4.6	21.2	0.3
nPDA-pH10	75.3	5.3	19.2	0.2

The membrane substrate roughness was also characterized using AFM. Table 2 shows the average root-mean-square surface roughness (R_{ms}) of the prepared polyketone and PDA-coated membrane substrates. The surface roughness of both pristine polyketone and sPDA samples showed statistically similar average R_{ms} values, with sPDA having a lower average, indicating how the conventional PDA coating could result in the formation of a smooth coating on top of the membrane substrate. The surface roughness, however, increased as pH increased during the self-polymerization of dopamine. The surface roughness was heavily influenced by the formation of the nano-sized PDA particles, which have been formed upon exposure of dopamine monomer with NH_3 initiator.

Table 2. Average root-mean-square roughness (R_{ms}) of the membrane substrates characterized using AFM.

Membrane substrate	Average Roughness, R_{ms} (nm)
Polyketone	59.3 ± 10.2
sPDA	48.2 ± 8.4
nPDA-pH8	96.6 ± 17.1
nPDA-pH9	129 ± 21.6
nPDA-pH10	160 ± 33.6

Figure 3(a) shows the contact angle measurements of the plain and PDA-modified polyketone substrates. Due to the functional groups present in the structure of PDA, the membrane substrate surfaces were also effectively functionalized upon coating and the hydrophilicity of the surfaces were effectively enhanced as well [37]. The effect of surface roughness also influenced the surface wettability of the

membrane substrates. The aggregation of nanoparticulate PDA on the membrane substrate surface effectively increased the surface roughness, as shown in Table 2. Aside from hydrophilicity, surface wettability is also influenced by the roughness, as given by the Wenzel equation [38]:

$$\cos\theta_{app} = r\cos\theta \quad (8)$$

where θ_{app}, θ, and r are the respectively apparent contact angle, actual contact angle on a perfectly smooth solid surface, and the ratio of the rough surface area and projected area. Thus, it is expected that a lower contact angle measurement would be obtained on a rougher surface.

It is also interesting to note that PDA modification of the membrane substrates resulted in smaller surface pores and narrower pore size distribution as shown in Figure 3. It was expected that PDA modification could cause partial blockage of the surface pores [31]. The number of surface pores decreased due to the introduction of the intermediate layer following the PDA polymerization. The nano-sized PDA particles were positioned on the support layer interface. Aggregated nano-sized particles were observed on the surface, as shown in Figure 2, which blocked the surface pores [22]. The PDA coating, however, makes up for the decrease in porosity by providing higher functionality and hydrophilicity to the membrane substrate. The bulk porosity of the membrane substrates were determined using gravimetric method, to account for the "wetted porosity" effect of PDA coating, as introduced by Arena et al. [39]. As shown in Figure 3(a), the bulk porosity of PK-sPDA substrate increased from that of the pristine PK substrate, as an effect of the PDA coating. The porous structure of the membrane substrates coated with nanoparticulate PDA exhibited lower bulk porosity values; however, this is mainly attributed to the partial blockage of the surface pores due to the growth of PDA nanoparticles. This was supported by the average surface pore size values shown in Figure 3(b).

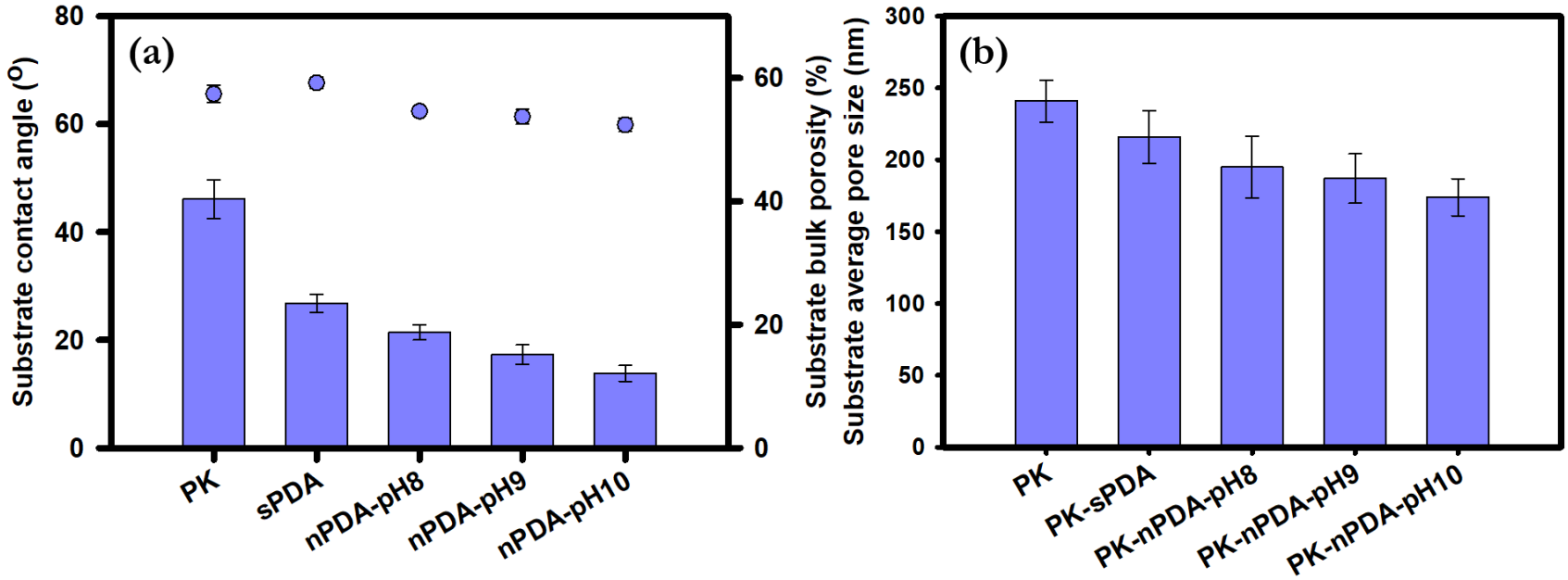

285

286 Figure 3. (a) Surface contact angle and bulk porosity and (b) average surface pore size of the pristine polyketone and polydopamine-coated

287 polyketone membrane substrates (measured using ImageJ software).

3.2. TFC membrane characterization

The morphology of the TFC membranes observed using FE-SEM are shown in Figure 4. Upon inspection of the polyamide surface morphology of the membrane samples (Figure 4(a)), it is interesting that the polyamide of the plain TFC and that with smooth PDA interlayer were observed to be highly dense, while the polyamide of the membranes with nanoparticle PDA interlayer were observed to be less dense, which may indicate the formation of looser polyamide structure. This difference in the morphology of the polyamide formed is highly attributed to the properties of the intermediate layer between the substrate and the polyamide layer. The polyamide selective layer formation resulted from the uniform distribution of the aqueous solution on the highly hydrophilic surface and the slower diffusion of MPD during IP as a result of the introduction of the intermediate layer [40]. Furthermore, the cross-section images show the changes in the morphology of the selective layers formed on top of the porous substrate. There was a noticeable change in the polyamide layer thickness for the samples. Polyamide has a typical thickness of 100 to 150 nm, and the measured thickness of the polyamide selective layer of the plain TFC membrane was well within this range. The same observation was true for the polyamide thickness of the TFC membrane with a smooth PDA interlayer; however, the polyamide layer of sPDA TFC was observed to be even thinner than that of the plain TFC membrane. This shows that the smooth PDA interlayer forms denser and thinner selective layers. Aside from being caused by the smoothness of the membrane substrate, this phenomenon is also most likely due to the ability of PDA to penetrate into the pores of the membrane substrate, enhancing its hydrophilicity [41] and improving the retention of the MPD precursor during IP, leading to the formation of denser, yet thinner polyamide [42]. On the other hand, there was an increase, albeit slightly, in the apparent polyamide thickness observed for the membranes modified with a nanoparticulate PDA interlayer.

Surface roughness of the TFC membranes was measured and shown in Figure 5(a). The surface roughness data support the membrane surface morphology shown from the FE-SEM images. The morphology of the substrate influenced the formation of the polyamide selective layer. The roughness of the membrane substrates coated with nanoparticulate PDA intermediate layer resulted in the formation of

rougher polyamide layer, and TFC membrane roughness increased as the pH of PDA polymerization increased. The R_{ms} values of the PK-nPDA samples were much greater than those of the pristine TFC and PK-sPDA TFC membranes. The polyamide selective layer surface roughness can be attributed to the presence of more ridge structures formed atop the particulate PDA intermediate layer. Membrane surface roughness is directly related to enhanced affinity to water, and tuning the membrane surface roughness could enhance the membrane permeability [43]. Membrane separation performance is highly dependent on the roughness of the polyamide selective layer, due to the increased surface filtration area [44]. The surface water contact angle of the TFC membranes was also measured and presented in Figure 5(b). Due to the relatively hydrophobic property of polyamide, the contact angle measurements of the TFC membranes were observed to increase from those of their substrate counterparts. The lowest contact angle measurement was observed for PK-nPDA-pH10 (47.2°), owing to the membrane surface roughness (Figure 5(a)).

To further characterize the polyamide selective layer of the TFC membranes and how its formation was influenced by the introduction of the intermediate layer, XPS analysis was performed to determine the atomic composition and degree of cross-linking of the polyamide layer in each membrane. Based on the atomic composition analysis, the ratio of O and N can provide the degree of cross-linkage of the polyamide layer. The O/N ratio is inversely proportional to the degree of cross-linkage, which can be calculated using:

$$a + b = 1 \quad (7)$$

$$\frac{O}{N} = \frac{3a+4b}{3a+2b} \quad (8)$$

where a and b are the fractions of the crosslinked structure and linear structure components of polyamide, respectively [45].

Table 3. Atomic composition and the degree of cross-linking of the polyamide selective layer of the TFC membranes.

Membrane	**C (%)**	**N (%)**	**O (%)**	**O/N**	***a* value**

Polyketone TFC	72.3	13.1	14.6	1.12	0.83
sPDA TFC	72.1	13.3	14.6	1.09	0.87
nPDA-pH8 TFC	71.7	12.8	15.5	1.21	0.72
nPDA-pH9 TFC	72.6	12.1	15.3	1.26	0.66
nPDA-pH10 TFC	73.0	11.7	15.3	1.30	0.61

Table 3 shows the atomic composition and fraction of cross-linking component of the polyamide layers of the TFC membranes prepared in this study. The XPS analysis shows and confirms that the introduction of intermediate PDA layer could influence formation of the polyamide selective layer. Both the pristine TFC and sPDA TFC membranes show a high degree of cross-linkage of 0.83 and 0.87, respectively, while those with nanoparticulate PDA intermediate layer exhibited lower degree of cross-linkage between 0.60 and 0.72. The presence of the embedded PDA nanoparticles increased roughness of the membrane substrate, causing a less even distribution of the MPD and TMC monomers during IP and resulting in lower degrees of cross-linkage. The lower degree of cross-linkage then explains the appearance of looser polyamide layer of the nPDA TFC membranes, as shown by the FE-SEM images (Figure 5).

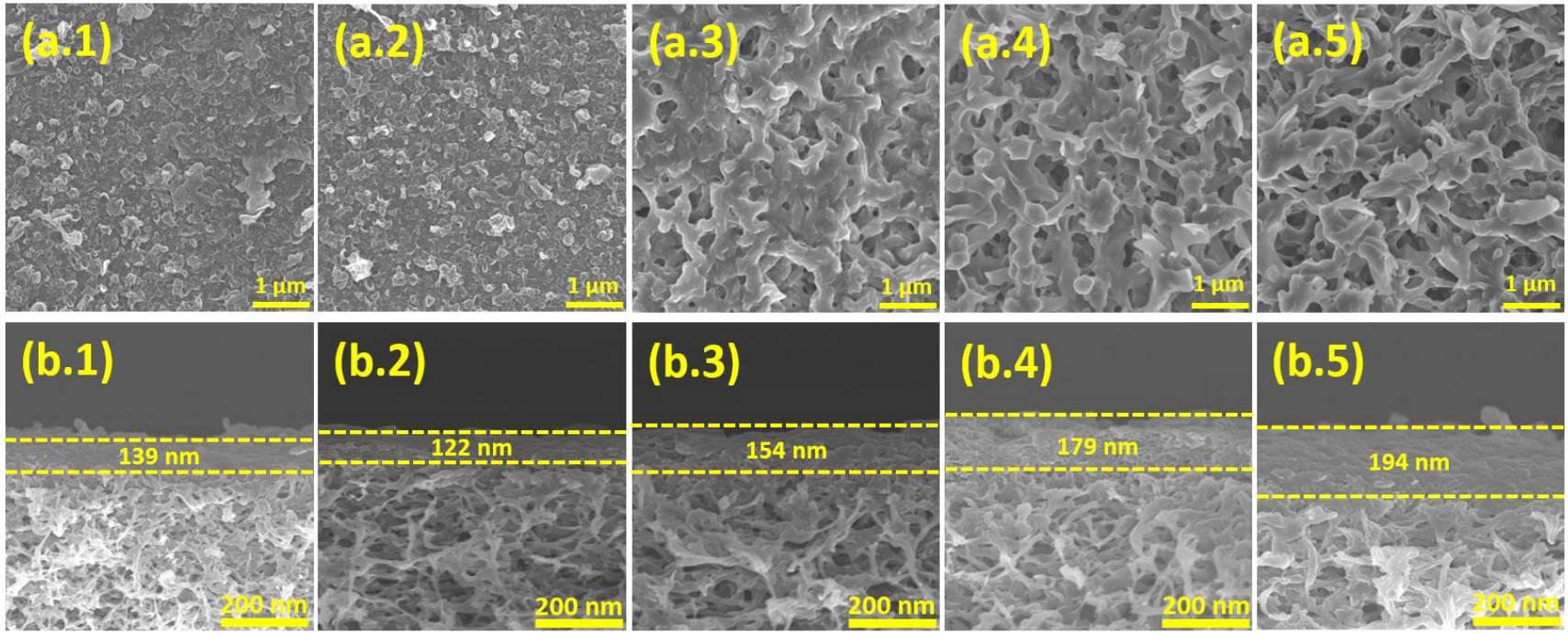

346

347 Figure 4. Polyamide selective layer (a) surface and (b) cross-section FE-SEM images of the TFC membranes: (1) plain TFC, (2) sPDA TFC, (3)
348 nPDA-pH8 TFC, (4) nPDA-pH9 TFC, and (5) nPDA-pH10 TFC. Polyamide layer thickness of the TFC membranes are indicated in each figure.

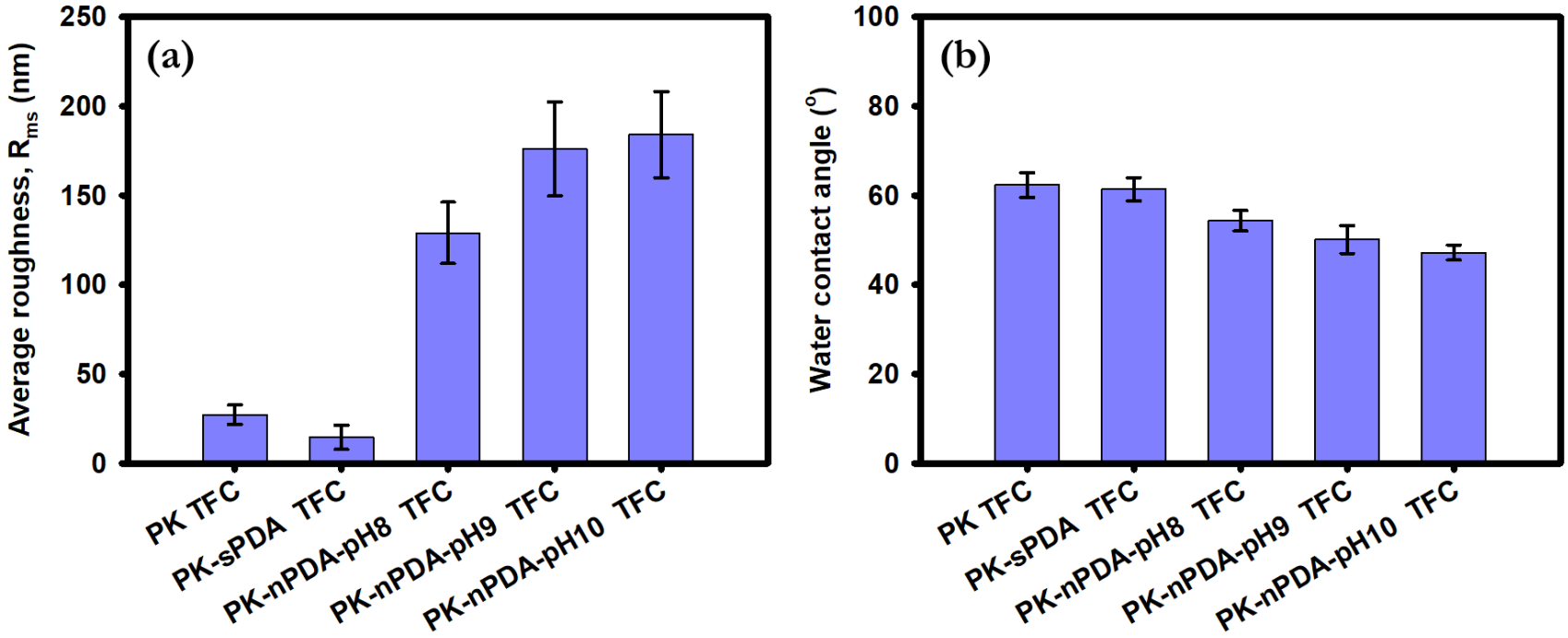

349

350 Figure 5. (a) Average root-mean-square surface roughness (R_{ms}) and (b) surface water contact angle of the TFC membranes.

3.3. Membrane intrinsic transport properties

The membrane intrinsic transport properties were evaluated and presented in Table 4.

Table 4. Intrinsic transport properties of the TFC membranes.

Membrane	*A* (L m^{-2} $h^{-1}$$bar^{-1}$)	*B* (L m^{-2} h^{-1})	*B/A* (bar)	*R* (%)	*S* (µm)
PK TFC	1.36 ± 0.13	0.33 ± 0.05	0.24	97.5 ± 0.3	212
PK-sPDA TFC	2.12 ± 0.08	0.39 ± 0.12	0.18	98.3 ± 0.4	198
PK-nPDA-pH8 TFC	2.58 ± 0.15	0.87 ± 0.18	0.34	95.3 ± 0.4	225
PK-nPDA-pH9 TFC	2.76 + 0.19	1.08 ± 0.11	0.39	94.7 ± 0.6	230
PK-nPDA-pH10 TFC	2.41 ± 0.23	1.44 ± 0.16	0.60	92.8 ± 0.8	247

The membranes exhibited higher water permeability (*A*) upon PDA modification, when compared to the plain TFC membrane. The water permeability increased for membranes with dopamine self-polymerization at higher pH (pH 8 to 9). However, the membrane modified with particulate PDA interlayer at pH 10 showed slightly lower water permeability which can most likely be explained because of the surface pore blockage due to the presence of the PDA nanoparticles [22]. The highest *A* value of 2.76 L m^{-2} h^{-1} bar^{-1} was observed for the PK-nPDA-pH9 TFC sample. The best water permeability is likely caused by the satisfactory coating on top of the membrane surface, without blocking the porous structure of the polyketone, while enhancing the surface hydrophilicity, and the presence of higher free volume of the looser polyamide thin film.

As expected, the increase in water permeability is accompanied with corresponding increase in solute permeability as indicated by the solute permeability (*B*) values in Table 4. The membranes with thinner and denser selective layers exhibited high solute rejection values, while those with looser, less cross-linked, and quite thicker polyamide layers exhibited a decrease in rejection and increase in solute permeability. Overall selectivity of the TFC membranes were given by the *B/A* values, which indicated that the TFC membranes suffered lower selectivity after formation of PDA interlayer at higher pH.

The structure parameter (*S* value) of the membranes were also determined and shown in Table 4. The introduction of the smooth PDA intermediate layer facilitated the formation of a thin, dense polyamide selective layer and the resultant TFC membrane was found to have a lower *S* value (198 μm) than the pristine TFC membrane (212 μm). The formation of nanoparticulate PDA intermediate layer, on the other hand, increased the *S* values within the range of 225-250 μm range.

3.4. Membrane osmotic performance and energy generation capability

Membrane performance for the PRO process was evaluated using DI water and 1.0 M NaCl as the FS and DS, respectively. The TFC membranes were first evaluated for forward osmosis (FO) performance. The water flux (J_w) was obtained after operation with two different membrane orientations: (a) active layer facing the DS (AL-DS) and (b) active layer facing the FS (AL-FS), and the results are shown in Figure 6. Without the application of hydraulic pressure, consistently with the pure water permeability data, PK-nPDA-pH9 TFC showed the highest initial water flux of 40.8 L m^{-2} h^{-1}, with a sharp flux decline at PK-nPDA-pH10 TFC. Comparison of the water flux values at both AL-DS and AL-FS membrane orientations could give light on the internal concentration polarization (ICP) occurring in the TFC membrane, which could dramatically decrease water flux. While all the J_w values were observed to be lower during AL-FS operation, it can be noted that the difference was smaller for the TFC membranes with PDA interlayer, which could indicate that the effect of ICP did not affect the membrane water permeability performance [46]. The water flux of the TFC membranes was observed to increase after the introduction of the PDA intermediate layer. In the case of the PK-sPDA TFC membrane, the formation of thinner, dense polyamide layer resulted in increased water permeability. On the other hand, the PK-nPDA TFC membranes had increased water flux values compared to pristine PK-TFC and PK-sPDA, due to the increased surface roughness and formation of looser polyamide selective layer. However, the observed flux decline for PK-nPDA-pH10 TFC could be attributed to the pore blockage within the membranes resulting from the aggregation of the nanoparticulate PDA.

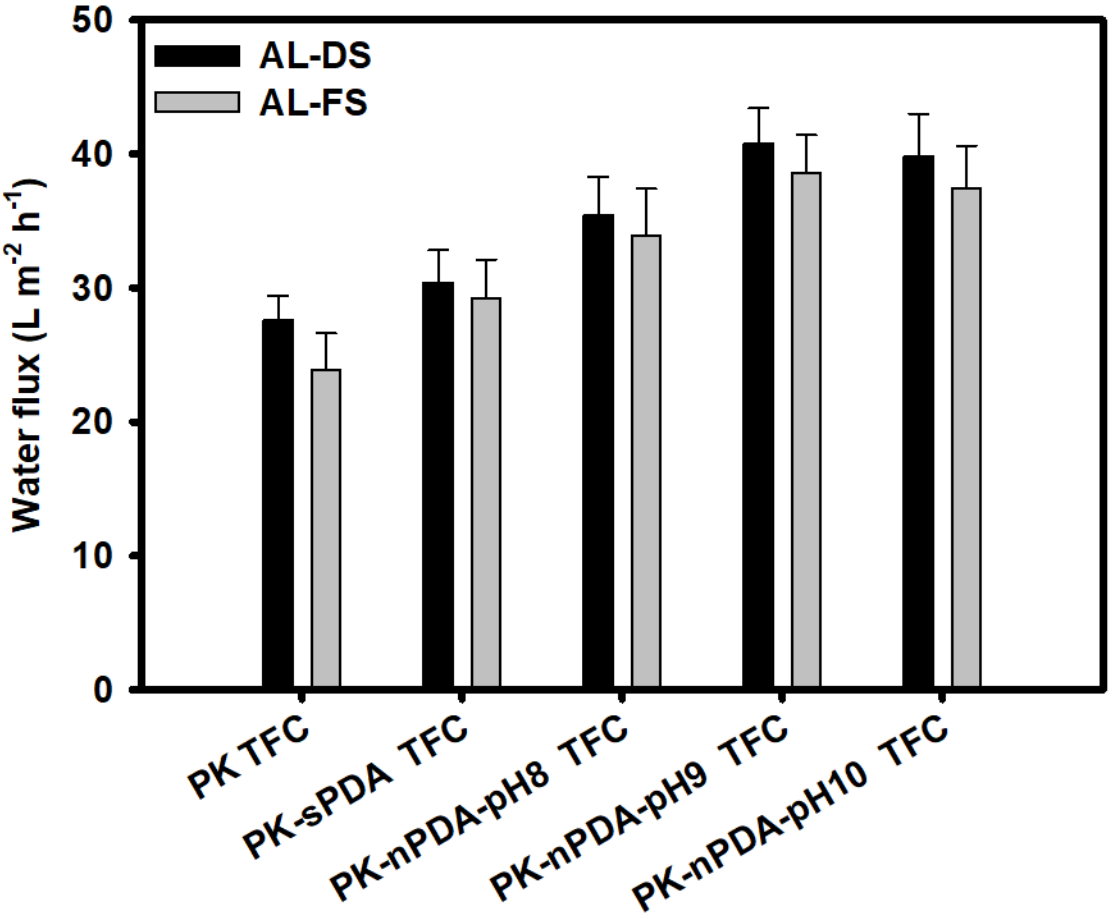

396

397 Figure 6. Water flux of the TFC membranes during forward osmosis (FO) operation at active layer facing
398 the draw solution (AL-DS) and active layer facing the feed solution (AL-FS) membrane orientations. (FS:
399 DI water; DS: 1.0 M NaCl).

400

401 Figure 7 shows the water flux, specific reverse salt flux ($J_s J_w^{-1}$, g L^{-1}), and power density (W m^{-2}) of
402 the TFC membranes at different applied pressures. Water flux dramatically increased upon the introduction
403 of the PDA interlayer, indicating the enhanced hydrophilicity of the membrane substrate, which facilitated
404 water transport. The highly hydrophilic nature of the intermediate layer complemented the microporous

structure of the polyketone membrane substrate, thereby resulting in better water transport during osmotic process.

The introduction of nanoparticulate PDA intermediate layer and the subsequent production of looser polyamide selective layer caused decline of the membrane selectivity and an increase of reverse salt diffusion during PRO process operation. These were not observed for the plain TFC membrane and the smooth PDA interlayer-modified TFC membrane, which both exhibited specific reverse salt flux values lower than 0.3 g L^{-1} for osmotic operation at minimal applied hydraulic pressure (Figure 7(b)). With the formation of looser polyamide atop the nanoparticulate PDA intermediate layer, even at minimal applied hydraulic pressure, the specific reverse salt flux increased dramatically to 0.45 g L^{-1} for nPDA-pH8 TFC and 0.87 g L^{-1} for PK-nPDA-pH10 TFC. As the applied pressure increased during PRO operation, the specific reverse salt flux values were observed to increase as well. The formation of nanoparticulate PDA intermediate layer significantly affected the selectivity of the TFC membranes; thus, the PDA nanoparticle formation should be optimized to enhance the water permeability, without sacrificing the membrane selectivity which may cause considerable loss of osmotic driving force by severe concentration polarization during operation [47].

In terms of power density, the highest power density of 17.1 W m^{-2} was obtained from PK-nPDA-pH-9 TFC at an applied hydraulic pressure of 25 bar as presented in Figure 7(c). The increase in the power density was dramatic compared to that of the plain TFC membrane, whose power density at 25 bar was only 8.6 W m^{-2}. Based on the increasing trend in the power density of the membranes as presented in Figure 6(c), the maximum power density has yet to be achieved. The membranes were not tested at applied pressure higher than 25 bar because of limitation with the mechanical strength of the membrane. This shows that with further optimization of the membrane mechanical strength, these membranes have the potential to achieve even higher power density at higher applied pressure.

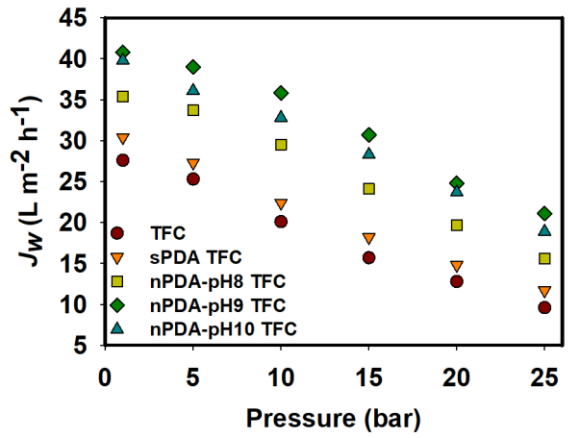

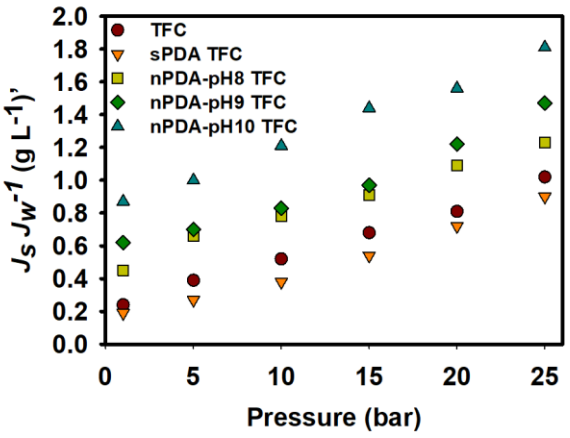

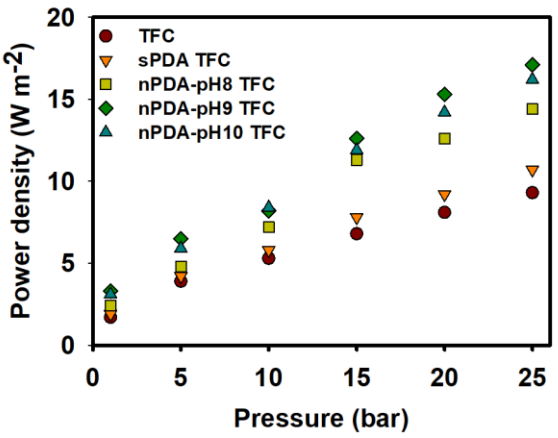

428

429 Figure 7. Osmotic performance, in terms of (a) water flux (J_w), (b) specific reverse salt flux ($J_s J_w^{-1}$), and
430 (c) power density, of the TFC membranes during PRO operation at different applied hydraulic pressures
431 using DI water as FS and 1.0 M NaCl as DS.

4. Conclusion

In this study, polydopamine (PDA) intermediate layer was formed in between the aliphatic polyketone membrane substrate and the polyamide selective layer of a pressure retarded osmosis (PRO) thin film composite (TFC) membrane. Two types of PDA interlayer were formed and compared: the conventional smooth PDA and particulate PDA. Furthermore, the effect of pH during the self-polymerization of dopamine was investigated and evaluated in terms of the ease of PDA nanoparticle formation and its subsequent effect to the polyamide formation during interfacial polymerization and the membrane performance during PRO process operation. The following conclusions can be drawn from this study:

1. The morphology of the PDA intermediate layer significantly influences the formation of polyamide selective layer. Both the pristine TFC and sPDA TFC (modified with smooth PDA interlayer) membranes exhibited highly dense and thinner polyamide layer, while those with the particulate PDA interlayer were observed to have formed looser and quite thicker polyamide layers.
2. Not only does the structure of the polyamide selective layer was affected by the intermediate layer morphology, the membrane performance was likewise affected. Introduction of the particulate PDA interlayer created more free volume and transport channels, which compensated the pore-blocking phenomenon of the nano-sized PDA particles. This resulted in higher water permeability for nPDA-pH8 TFC and nPDA-pH9 TFC. However, for nPDA-pH10 TFC, the more alkaline environment during dopamine self-polymerization resulted in better nucleation of the PDA nanoparticles, which as evidenced by the membrane characterization techniques.
3. The looser polyamide selective layer formed on top of the particulate PDA intermediate layer also led to slight decrease in the membrane selectivity, compared with the pristine and sPDA TFC samples.
4. The membrane performance was evaluated using deionized water and 1.0 M NaCl as feed and draw solutions, respectively. The TFC membrane with nanoparticulate PDA layer formed at pH 9.0

exhibited the best initial water flux of 40.8 L m^{-2} h^{-1}, and this membrane also showed the highest power density of 17.1 W m^{-2} at 25 bar.

This study was able to prove that a simple, facile, and versatile technique such as the ammonia-initialized introduction of nanoparticulate PDA intermediate layer, at controlled conditions, could significantly improve the water transport properties of a TFC membrane, while maintaining satisfactory rejection ability.

Acknowledgments

This research was made possible by a grant from the Qatar National Research Fund under its National Priorities Research Program award number NPRP 10-1231-160069. The paper's contents are solely the responsibility of the authors and do not necessarily represent the official views of the Qatar National Research Fund.

References

[1] A. Achilli, A.E. Childress, Pressure retarded osmosis: From the vision of Sidney Loeb to the first prototype installation - Review, Desalination, 261 (2010) 205-211.

[2] R.R. Gonzales, S.-H. Kim, Dark fermentative hydrogen production following the sequential dilute acid pretreatment and enzymatic saccharification of rice husk, International Journal of Hydrogen Energy, 42 (2017) 27577-27583.

[3] C. Klaysom, T.Y. Cath, T. Depuydt, I.F.J. Vankelecom, Forward and pressure retarded osmosis: potential solutions for global challenges in energy and water supply, Chemical Society Reviews, 42 (2013) 6959-6989.

[4] F. Volpin, R.R. Gonzales, S. Lim, N. Pathak, S. Phuntsho, H.K. Shon, GreenPRO: A novel fertiliser-driven osmotic power generation process for fertigation, Desalination, 447 (2018) 158-166.

[5] A. Achilli, T.Y. Cath, A.E. Childress, Power generation with pressure retarded osmosis: An experimental and theoretical investigation, Journal of Membrane Science, 343 (2009) 42-52.

[6] S. Loeb, Large-scale power production by pressure-retarded osmosis, using river water and sea water passing through spiral modules, Desalination, 143 (2002) 115-122.

[7] S.-P. Sun, T.-S. Chung, Outer-selective pressure-retarded osmosis hollow fiber membranes from vacuum-assisted interfacial polymerization for osmotic power generation, Environmental Science & Technology, 47 (2013) 13167-13174.

[8] X. Liu, L.-X. Foo, Y. Li, J.-Y. Lee, B. Cao, C.Y. Tang, Fabrication and characterization of nanocomposite pressure retarded osmosis (PRO) membranes with excellent anti-biofouling property and enhanced water permeability, Desalination, 389 (2016) 137-148.

[9] L. Zhang, Q. She, R. Wang, S. Wongchitphimon, Y. Chen, A.G. Fane, Unique roles of aminosilane in developing anti-fouling thin film composite (TFC) membranes for pressure retarded osmosis (PRO), Desalination, 389 (2016) 119-128.

[10] N.Y. Yip, A. Tiraferri, W.A. Phillip, J.D. Schiffman, L.A. Hoover, Y.C. Kim, M. Elimelech, Thin-film composite pressure retarded osmosis membranes for sustainable power generation from salinity gradients, Environmental Science & Technology, 45 (2011) 4360-4369.

[11] S.J. Moon, S.M. Lee, J.H. Kim, S.H. Park, H.H. Wang, J.H. Kim, Y.M. Lee, A highly robust and water permeable thin film composite membranes for pressure retarded osmosis generating 26 W·m−2 at 21 bar, Desalination, 483 (2020) 114409.

[12] R.R. Gonzales, M.J. Park, T.-H. Bae, Y. Yang, A. Abdel-Wahab, S. Phuntsho, H.K. Shon, Melamine-based covalent organic framework-incorporated thin film nanocomposite membrane for enhanced osmotic power generation, Desalination, 459 (2019) 10-19.

[13] R.R. Gonzales, Y. Yang, M.J. Park, T.-H. Bae, A. Abdel-Wahab, S. Phuntsho, H.K. Shon, Enhanced water permeability and osmotic power generation with sulfonate-functionalized porous polymer-incorporated thin film nanocomposite membranes, Desalination, 496 (2020) 114756-114765.

[14] P.G. Ingole, W. Choi, K.H. Kim, C.H. Park, W.K. Choi, H.K. Lee, Synthesis, characterization and surface modification of PES hollow fiber membrane support with polydopamine and thin film composite for energy generation, Chemical Engineering Journal, 243 (2014) 137-146.

[15] H. Lee, S.M. Dellatore, W.M. Miller, P.B. Messersmith, Mussel-inspired surface chemistry for multifunctional coatings, Science, 318 (2007) 426.

[16] S. Kasemset, A. Lee, D.J. Miller, B.D. Freeman, M.M. Sharma, Effect of polydopamine deposition conditions on fouling resistance, physical properties, and permeation properties of reverse osmosis membranes in oil/water separation, Journal of Membrane Science, 425-426 (2013) 208-216.

[17] H. Guo, Z. Yao, J. Wang, Z. Yang, X. Ma, C.Y. Tang, Polydopamine coating on a thin film composite forward osmosis membrane for enhanced mass transport and antifouling performance, Journal of Membrane Science, 551 (2018) 234-242.
[18] J.-H. Jiang, L.-P. Zhu, H.-T. Zhang, B.-K. Zhu, Y.-Y. Xu, Improved hydrodynamic permeability and antifouling properties of poly(vinylidene fluoride) membranes using polydopamine nanoparticles as additives, Journal of Membrane Science, 457 (2014) 73-81.
[19] Y. Li, Y. Su, X. Zhao, X. He, R. Zhang, J. Zhao, X. Fan, Z. Jiang, Antifouling, high-flux nanofiltration membranes enabled by dual functional polydopamine, ACS Applied Materials & Interfaces, 6 (2014) 5548-5557.
[20] L. Zhang, Y. Lin, S. Wang, L. Cheng, H. Matsuyama, Engineering of ultrafine polydopamine nanoparticles in-situ assembling on polyketone substrate for highly-efficient oil-water emulsions separation, Journal of Membrane Science, 613 (2020) 118501.
[21] L. Zhang, R. Takagi, S. Wang, Y. Lin, K. Guan, L. Cheng, H. Matsuyama, In situ formation of ultrathin polyampholyte layer on porous polyketone membrane via a one-step dopamine co-deposition strategy for oil/water separation with ultralow fouling, Journal of Membrane Science, 619 (2021) 118789.
[22] H.-g. Choi, A.A. Shah, S.-E. Nam, Y.-I. Park, H. Park, Thin-film composite membranes comprising ultrathin hydrophilic polydopamine interlayer with graphene oxide for forward osmosis, Desalination, 449 (2019) 41-49.
[23] Y. Lv, Y. Du, W.-Z. Qiu, Z.-K. Xu, Nanocomposite membranes via the codeposition of polydopamine/ polyethylenimine with silica nanoparticles for enhanced mechanical strength and high water permeability, ACS Applied Materials & Interfaces, 9 (2017) 2966-2972.
[24] Y. Mu, K. Zhu, J. Luan, S. Zhang, C. Zhang, R. Na, Y. Yang, X. Zhang, G. Wang, Fabrication of hybrid ultrafiltration membranes with improved water separation properties by incorporating environmentally friendly taurine modified hydroxyapatite nanotubes, Journal of Membrane Science, 577 (2019) 274-284.
[25] A.A. Shah, Y.H. Cho, H.-g. Choi, S.-E. Nam, J.F. Kim, Y. Kim, Y.-I. Park, H. Park, Facile integration of halloysite nanotubes with bioadhesive as highly permeable interlayer in forward osmosis membranes, Journal of Industrial and Engineering Chemistry, 73 (2019) 276-285.
[26] M. Wu, J. Yuan, H. Wu, Y. Su, H. Yang, X. You, R. Zhang, X. He, N.A. Khan, R. Kasher, Z. Jiang, Ultrathin nanofiltration membrane with polydopamine-covalent organic framework interlayer for enhanced permeability and structural stability, Journal of Membrane Science, 576 (2019) 131-141.
[27] M.J. Park, S. Lim, R.R. Gonzales, S. Phuntsho, D.S. Han, A. Abdel-Wahab, S. Adham, H.K. Shon, Thin-film composite hollow fiber membranes incorporated with graphene oxide in polyethersulfone support layers for enhanced osmotic power density, Desalination, 464 (2019) 63-75.
[28] D.L. Zhao, S. Das, T.-S. Chung, Carbon quantum dots grafted antifouling membranes for osmotic power generation via pressure-retarded osmosis process, Environmental Science & Technology, 51 (2017) 14016-14023.
[29] W. Gai, D.L. Zhao, T.-S. Chung, Novel thin film composite hollow fiber membranes incorporated with carbon quantum dots for osmotic power generation, Journal of Membrane Science, 551 (2018) 94-102.
[30] Y. Kim, E. Yang, H. Park, H. Choi, Anti-biofouling effect of a thin film nanocomposite membrane with a functionalized-carbon-nanotube-blended polymeric support for the pressure-retarded osmosis process, RSC Advances, 10 (2020) 5697-5703.
[31] G. Han, S. Zhang, X. Li, N. Widjojo, T.-S. Chung, Thin film composite forward osmosis membranes based on polydopamine modified polysulfone substrates with enhancements in both water flux and salt rejection, Chemical Engineering Science, 80 (2012) 219-231.
[32] C. Liu, R. Takagi, T. Shintani, L. Cheng, K.L. Tung, H. Matsuyama, Organic liquid mixture separation using an aliphatic polyketone-supported polyamide organic solvent reverse osmosis (OSRO) membrane, ACS Applied Materials & Interfaces, 12 (2020) 7586-7594.

[33] Y. Sun, L. Cheng, T. Shintani, Y. Tanaka, T. Takahashi, T. Itai, S. Wang, L. Fang, H. Matsuyama, Development of high-flux and robust reinforced aliphatic polyketone thin-film composite membranes for osmotic power generation: Role of reinforcing materials, Industrial & Engineering Chemistry Research, 57 (2018) 13528-13538.
[34] R.R. Gonzales, M.J. Park, L. Tijing, D.S. Han, S. Phuntsho, H.K. Shon, Modification of nanofiber support layer for thin film composite forward osmosis membranes via layer-by-layer polyelectrolyte deposition, Membranes, 8 (2018) 70-84.
[35] S.J. Kwon, S.-H. Park, M.G. Shin, M.S. Park, K. Park, S. Hong, H. Park, Y.-I. Park, J.-H. Lee, Fabrication of high performance and durable forward osmosis membranes using mussel-inspired polydopamine-modified polyethylene supports, Journal of Membrane Science, 584 (2019) 89-99.
[36] L. Zhang, Y. Lin, H. Wu, L. Cheng, Y. Sun, T. Yasui, Z. Yang, S. Wang, T. Yoshioka, H. Matsuyama, An ultrathin in situ silicification layer developed by an electrostatic attraction force strategy for ultrahigh-performance oil–water emulsion separation, Journal of Materials Chemistry A, 7 (2019) 24569-24582.
[37] J.T. Arena, S.S. Manickam, K.K. Reimund, B.D. Freeman, J.R. McCutcheon, Solute and water transport in forward osmosis using polydopamine modified thin film composite membranes, Desalination, 343 (2014) 8-16.
[38] L. Zhang, R. Rolly Gonzales, T. Istirokhatun, Y. Lin, J. Segawa, H. Kyong Shon, H. Matsuyama, In situ engineering of an ultrathin polyamphoteric layer on polyketone-based thin film composite forward osmosis membrane for comprehensive anti-fouling performance, Separation and Purification Technology, 272 (2021) 118922.
[39] J.T. Arena, B. McCloskey, B.D. Freeman, J.R. McCutcheon, Surface modification of thin film composite membrane support layers with polydopamine: Enabling use of reverse osmosis membranes in pressure retarded osmosis, Journal of Membrane Science, 375 (2011) 55-62.
[40] X. Yang, Y. Du, X. Zhang, A. He, Z.-K. Xu, Nanofiltration membrane with a mussel-inspired interlayer for improved permeation performance, Langmuir, 33 (2017) 2318-2324.
[41] H.-C. Yang, K.-J. Liao, H. Huang, Q.-Y. Wu, L.-S. Wan, Z.-K. Xu, Mussel-inspired modification of a polymer membrane for ultra-high water permeability and oil-in-water emulsion separation, Journal of Materials Chemistry A, 2 (2014) 10225-10230.
[42] A.K. Ghosh, E.M.V. Hoek, Impacts of support membrane structure and chemistry on polyamide-polysulfone interfacial composite membranes, Journal of Membrane Science, 336 (2009) 140-148.
[43] X. Ma, Z. Yang, Z. Yao, H. Guo, Z. Xu, C.Y. Tang, Tuning roughness features of thin film composite polyamide membranes for simultaneously enhanced permeability, selectivity and anti-fouling performance, Journal of Colloid and Interface Science, 540 (2019) 382-388.
[44] X. Song, B. Gan, Z. Yang, C.Y. Tang, C. Gao, Confined nanobubbles shape the surface roughness structures of thin film composite polyamide desalination membranes, Journal of Membrane Science, 582 (2019) 342-349.
[45] M.J. Park, C. Wang, D.H. Seo, R.R. Gonzales, H. Matsuyama, H.K. Shon, Inkjet printed single walled carbon nanotube as an interlayer for high performance thin film composite nanofiltration membrane, Journal of Membrane Science, (2020) 118901.
[46] X. Song, Y. Zhang, H.M. Abdel-Ghafar, E.-S.A. Abdel-Aal, M. Huang, S. Gul, H. Jiang, Polyamide membrane with an ultrathin GO interlayer on macroporous substrate for minimizing internal concentration polarization in forward osmosis, Chemical Engineering Journal, 412 (2021) 128607.
[47] Q. She, X. Jin, C.Y. Tang, Osmotic power production from salinity gradient resource by pressure retarded osmosis: Effects of operating conditions and reverse solute diffusion, Journal of Membrane Science, 401 (2012) 262-273.